Diel vertical migration: a diagnostic for variability of wind forcing over the Beaufort and Chukchi Seas

Stephen Okkonen
University of Alaska Fairbanks
Fairbanks, Alaska 99775
srokkonen@alaska.edu

Carin Ashjian
Woods Hole Oceanographic Institution
Woods Hole, Massachusetts 02543
cashjian@whoi.edu

Robert G. Campbell
University of Rhode Island
Narragansett, Rhode Island 02882
rgcampbell@uri.edu

Philip Alatalo
Woods Hole Oceanographic Institution
Woods Hole, Massachusetts 02543
palatalo@whoi.edu

Corresponding author:
Stephen Okkonen
Institute of Marine Science
University of Alaska Fairbanks
Fairbanks, Alaska 99775
srokkonen@alaska.edu
907-283-3234

Abstract

Measurements of echo intensities were acquired in shelf waters of the western Beaufort Sea near Utqiaġvik (formerly Barrow), Alaska by upward-looking 307 kHz acoustic Doppler current profilers during a 2008-2015 series of late-summer mooring deployments. These echo signals were analyzed for characteristic patterns of krill diel vertical migration (DVM) from which daily and seasonally-averaged DVM indices (DVMI) were derived. Time varying relationships among DVMIs (inferred krill biomasses) and local and regional wind regimes were diagnosed statistically. The threshold wind speed at which easterly winds promote upwelling of krill onto the western Beaufort shelf occurs at about 6 m s^{-1}. Inferred krill biomass increases on the shelf as upwelling winds relax. Years (2009, 2012) in which inferred krill biomasses were higher on the western Beaufort shelf occurred when average mid-summer winds over the Chukchi Sea were from the south and average late-summer winds over the Beaufort shelf were weak and variable. In contrast, years (2008, 2010-11, 2013-15) in which inferred krill biomasses were lower occurred when average mid-summer winds over the Chukchi Sea were weak and variable and average late-summer winds over the Beaufort shelf were generally easterly and strong.

Keywords: BEAUFORT SEA; CHUKCHI SEA; ZOOPLANKTON; DIEL VERTICAL MIGRATION; ADCP; WINDS; UPWELLING

1. Introduction

The Bering-Chukchi-Beaufort population of bowhead whales (*Balaena mysticetus)* often pause during their fall migration to forage on the western Beaufort shelf near Utqiaġvik (formerly Barrow), Alaska (Moore et al., 2000), a core-use area for these whales (Citta et al., 2015). Stomach analyses of bowheads harvested near Utqiaġvik indicate that, in most years, the principal prey consumed are euphausiids (krill), although copepods, mysids and amphipods are also found in their stomachs (Lowry et al., 2004; Moore et al., 2010). Krill encountered in the vicinity of Utqiaġvik originate in the Bering Sea (Berline et al., 2008). Of the three main schematized circulation pathways by which Pacific-origin waters cross the Chukchi Sea (Spall, 2007; Brugler et al., 2014), the targeting of relatively cool, saline waters by bowheads during their fall migration across the Chukchi shelf (Citta et al., 2018) implies that krill are preferentially carried northward along pathways in the western and central Chukchi Sea. These two pathways turn eastward over the northern Chukchi shelf ultimately carrying krill into Barrow Canyon and the Arctic Ocean. Berline et al. (2008) used a numerical circulation model to show that year-to-year differences in summer winds over the Chukchi Sea contribute to year-to-year differences in krill numbers at Utqiaġvik in autumn. According to a conceptual model developed by Ashjian et al. (2010) based on two late-summer field seasons (2005-2006), locally favorable foraging conditions for bowheads near Utqiaġvik initially require that easterly, upwelling winds move krill from the Beaufort slope onto the shelf. When the upwelling winds relax, the krill are retained and aggregated on the western Beaufort shelf where the prevailing westward-flowing shelf currents converge with the northeastward-flowing Alaskan Coastal Current in the vicinity of the eastern edge of Barrow Canyon. Ashjian et al. (2013) later

characterized this phenomenon of krill retention and aggregation as a 'krill trap'. Ashjian et al. (2010) additionally reported that large bowhead groups were observed 2-3 days following upwelling-favorable winds, suggesting that the krill-trap occurs as a lagged response to the relaxation of upwelling winds. Were upwelling winds to persist, the krill would be carried off-shelf into the deeper waters of Barrow Canyon (Ashjian et al., 2010; Okkonen et al., 2011). Proxy evidence for the krill trap is both behavioral and physical. In the former case, aerial surveys indicate that bowhead whales are more likely to exhibit feeding behavior in larger groups on the shelf during periods of relaxed winds (krill-trap winds) than during upwelling winds (Mocklin et al., 2011; Okkonen et al., 2011). In the latter case, Okkonen et al. (2011) used current velocities and satellite imagery to show that fronts/convergence zones occur in shelf waters near the eastern edge of Barrow Canyon during krill-trap winds, but are absent during upwelling winds and that the transition between these two regimes occurs at easterly wind velocities between 4.4 m s^{-1} and 6.6 m s^{-1}. An independent estimate of this threshold wind velocity, based on current reversals and salinity increases at the Beaufort shelf break, was reported by Schulze and Pickart (2012) who determined that about two-thirds of easterly wind events exceeding 4-7 m s^{-1} resulted in significant upwelling.

This summary understanding of krill availability at Utqiaġvik incorporates multiple krill biomass/abundance proxies (numerical, oceanographic and bowhead foraging behaviors) that vary in response to changes in regional or local winds. These wind-krill proxy relationships imply that a suitable multi-year observational record of krill itself potentially has encoded in it temporal and geographic characteristics of wind forcing that can be ascertained. Our broad goal is to investigate this implication. To do so, we draw upon an eight-season (2008-2015) record of

acoustic echo intensities measured by a series of 307 kHz ADCP-instrumented oceanographic moorings deployed as components of the multidisciplinary Bowhead Whale Feeding Ecology Study (e.g. Shelden and Mocklin, 2013) and a subsequent Arctic Observing Network program near Utqiaġvik. These deployments were used to acoustically monitor late-summer krill prey potentially available to bowhead whales on the western Beaufort shelf.

Active acoustic instruments such as ADCPs have long been used to characterize zooplankton behavior and estimate zooplankton biomass/abundance from acoustic backscatter (e.g. Flagg and Smith, 1989; Ashjian et al., 1994; Heywood, 1996; Ashjian et al., 1998; Tarling et al., 2002; Berge et al., 2009). The 307 kHz ADCP, in particular, has been used to investigate how diel vertical migration behavior of Arctic and sub-Arctic krill (*Thysanoessa* spp.) varies seasonally (Cottier et al., 2006) and how it is reflected in krill distribution and aggregation (Sourisseau et al., 2008). Although ADCP-measured volume backscatter is proportional to the biomass of scatterers in the water column and usually is ground-truthed using instrument specific calibrations and comparison with coincident volume backscatter estimated from size- and taxon-specific net-collected zooplankton and acoustic backscatter models (e.g., Lawson et al. 2004), we did not attempt to estimate krill biomass from our ADCP acoustic measurements or volume backscatter from coincident net tows because our net sampling methodology was not consistent across all survey years nor were net tows conducted in the vicinity of the moorings in all survey years.

Our investigation of the encoding of local and remote wind forcing into intra-seasonal and interannual differences in (inferred) krill prey biomass within the Utqiaġvik-area bowhead whale feeding hotspot is predicated on two key assumptions:

1) The DVM patterns recorded in the echo intensity data at our mooring sites are largely attributable to krill. We base this assumption on the known zooplankton composition of the shelf (e.g., Smoot and Hopcroft, 2017), which is comprised of small, low biomass, low backscatter taxa that do not exhibit DVM, the findings in Ashjian et al. (2010) in which krill are brought onto the inner shelf by upwelling, and the results of Lowry et al. (2004) and Moore et al. (2010) who reported that krill are the principal prey found in the stomachs of bowheads harvested on the shelf near Utqiaġvik.
2) Indices derived from DVM patterns, as described below, describe *relative* differences in late-summer krill biomasses on the western Beaufort shelf across survey seasons and across survey years.

These two assumptions mitigate the need for calibrating the measured echo intensities with independent measurements of water column scatterers (e.g. zooplankton, suspended sediments, detritus, air bubbles, etc.; the latter of which do not exhibit DVM) in the vicinity of the moorings.

Our paper is organized as follows. Section 2 begins with outlines of our study area and details of our mooring program. These are followed by descriptions of basic signal processing and statistical techniques used to derive daily and seasonal DVM indices (DVMI) from ADCP-measured acoustic intensities. Section 3 summarizes the DVMI-based diagnoses of temporal, geographic and amplitude characteristics of wind forcing regimes that influence krill biomass

availability on the western Beaufort shelf. In Sections 4 and 5, we compare our results with those from other studies, discuss alternate analytical strategies and present concluding statements.

2. Data and Methods

2.1 Setting

Our Utqiaġvik-area study domain (Fig. 1 inset) resides within the Pacific-Arctic region, here defined as being bounded by the 160°E and 120°W meridians and the 55°N and 80°N parallels. The Pacific-Arctic region encompasses much of the Bering Sea in the south and the East Siberian, Chukchi, and Beaufort Seas in the north (Fig. 1).

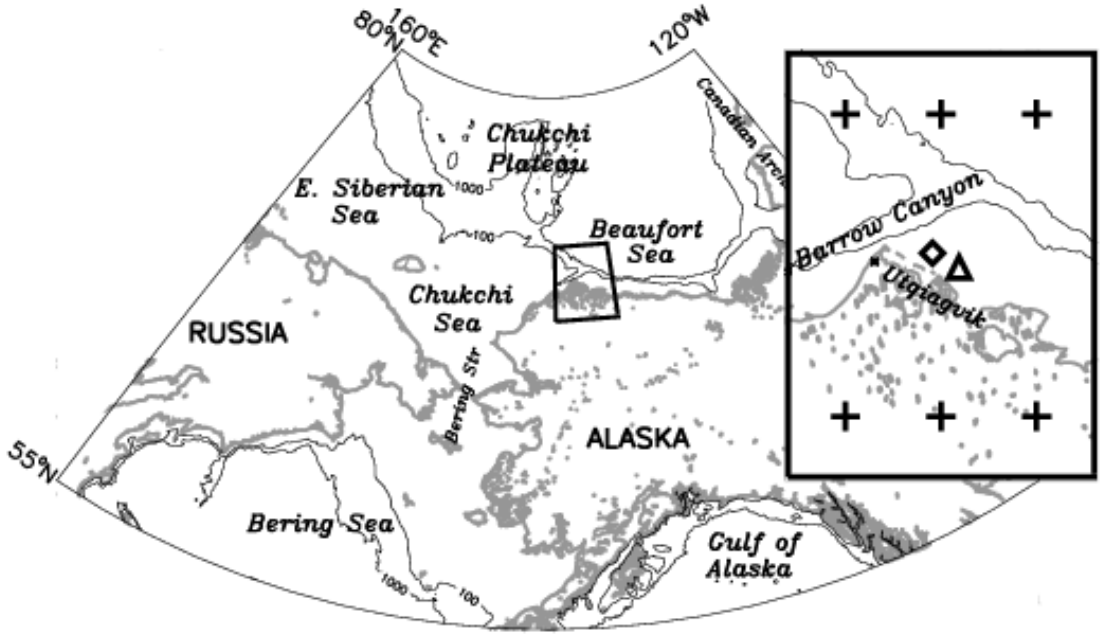

Fig. 1 *The Pacific-Arctic region with place names. The inset shows the Utqiaġvik-area study area. The 100-m and 1000-m isobaths are shown as thin black lines. The triangle in the inset shows the location of the 2008 mooring deployment on the western Beaufort shelf. The diamond shows the location of the 2009-2015 mooring deployments. The plus symbols identify NCEP grid points from which daily zonal winds were averaged to obtain a working dataset of local zonal winds.*

169

170 *2.2 Meteorological data*

171 NCEP/NCAR (National Centers for Environmental Prediction/National Center for Atmospheric
172 Research) Reanalysis daily surface wind and sea level pressure (SLP) data (Kalnay et al., 1996)
173 within the domain bounded by 55°N-80°N and 160°E-120°W were retained for regional
174 analyses. We adapt the metric of directional constancy from Moore (2003), here defined as the
175 ratio of the N-day vector mean wind speed to the N-day scalar mean wind speed, to characterize
176 winds on a variable-to-prevailing scale. Directional constancy values closer to zero indicate
177 winds exhibiting greater variability in their directions. Values closer to one indicate winds
178 exhibiting greater constancy in the direction of the mean wind (i.e. prevailing winds). Because
179 prevailing winds in the vicinity of the mooring locations are from the eastern quadrant (Pickart et
180 al., 2009; Okkonen et al., 2011), daily zonal (east-west; U) winds at the six nearest NCEP grid
181 points surrounding the mooring locations (see Fig. 1 inset) were averaged to provide a working
182 dataset of 2008-2015 daily local winds which is used to identify a threshold for upwelling winds.

183

184 *2.3 Moorings*

185 In late August 2008-2015, low-profile, bottom-mounted oceanographic moorings instrumented
186 with upward-looking 307 kHz Teledyne RD Instruments ADCPs were deployed in ~19 m of
187 water at locations within a bowhead whale core-use feeding area (Ashjian et al., 2010; Citta et al,
188 2015) on the western Beaufort shelf about 70 km (2008) and 45 km (2009-2015) east of Point
189 Barrow (Fig. 1 inset), respectively. These moorings were typically recovered a few weeks later
190 in early-to-mid September prior to the onset of the fall whaling season at Utqiaġvik. The ADCPs
191 returned usable measurements of echo intensities throughout the water column in twenty-seven

192 0.5-m depth cells from ~3.5 m above the bottom to within ~2.5 m of the surface at 15-minute or
193 20-minute intervals. Echo data were then linearly interpolated to 30-minute intervals. Exclusive
194 of partial days, the late summer 2008-2015 echo intensity record spans 180 days. Details of the
195 mooring deployments are summarized in Supplementary Table S1.
196
197 *2.4 Acoustic Doppler Current Profiler Echo Intensity data*
198 The echo intensity, *I*, of the acoustic signal received by an ADCP can be approximated as
199 (Deines, 1999),
200
201 $$I(t,z) = k_c E(t,z) = S_v(t,z) - C + L_{DBM} + P_{DBW} + k_c E_r - 10\,log_{10}((T_x+273.16)R^2) - 2\alpha R \quad (1)$$
202
203 in which
204 k_c is a scale factor (provided by Teledyne RDI) which converts returned signal strength indicator
205 (RSSI) counts to dB,
206 E is the RSSI amplitude (counts) from the ADCP in depth cell z and at time t,
207 S_v is the backscatter signal (dB) from targets of interest (i.e. zooplankton) and other scatterers
208 (e.g. detritus, air bubbles),
209 C is an empirical constant,
210 L_{DBM} is the $10\log_{10}$ (transmit pulse length, meters),
211 P_{DBW} is the $10\log_{10}$ (transmit power, watts),
212 E_r is a reference level RSSI (instrument noise) typically chosen to be the minimum recorded
213 value of E,
214 T_x is the transducer temperature (°C),

215 R is the slant range distance from the ADCP transducer to the depth cell (m), and

216 α is the attenuation coefficient of sound in water (m^{-1}).

217

218 For relatively cool temperatures encountered at the Beaufort shelf mooring locations (T_x < 6°C

219 for all seasonal deployments), the beam spreading term ($10\ log_{10}((T_x+273.16)R^2)$) is effectively a

220 function of slant range only and, for relatively short deployment durations (weeks), the source

221 terms (L_{DBM} and P_{DBW}) are effectively constant. Consequently, Equation 1 can be further

222 simplified to

223

224 $$I(t,z) = S_v(t,z) + C_1 - C_2(z) \quad (2)$$

225

226 in which source (power and instrument noise) terms are incorporated in C_1 (= $-C + L_{DBM} + P_{DBW}$

227 + $k_c E_r$) and loss terms (beam spreading and attenuation) are incorporated in C_2 (= 10

228 $log_{10}((T_x+273.16)R^2) + 2\alpha R$). In this formulation, temporal variability of the received echo

229 signal from a given depth cell (i.e. at a given slant range) depends only on temporal variability of

230 the scattering field in that depth cell.

231

232 To illustrate, consider a three-day (2-4 September 2012) subset from the eight-season record of

233 echo intensities, $I(z,t)$ (Fig. 2A). The acoustic backscatter environment on the shallow western

234 Beaufort shelf exhibits considerable variability with depth and with time. Elevated echo

235 intensities associated with the characteristic patterns of vertically migrating zooplankton are

236 evident on 2 September and 3 September. These DVM patterns show zooplankton beginning

237 their ascent through the water column as daylight wanes during the hours before local midnight.

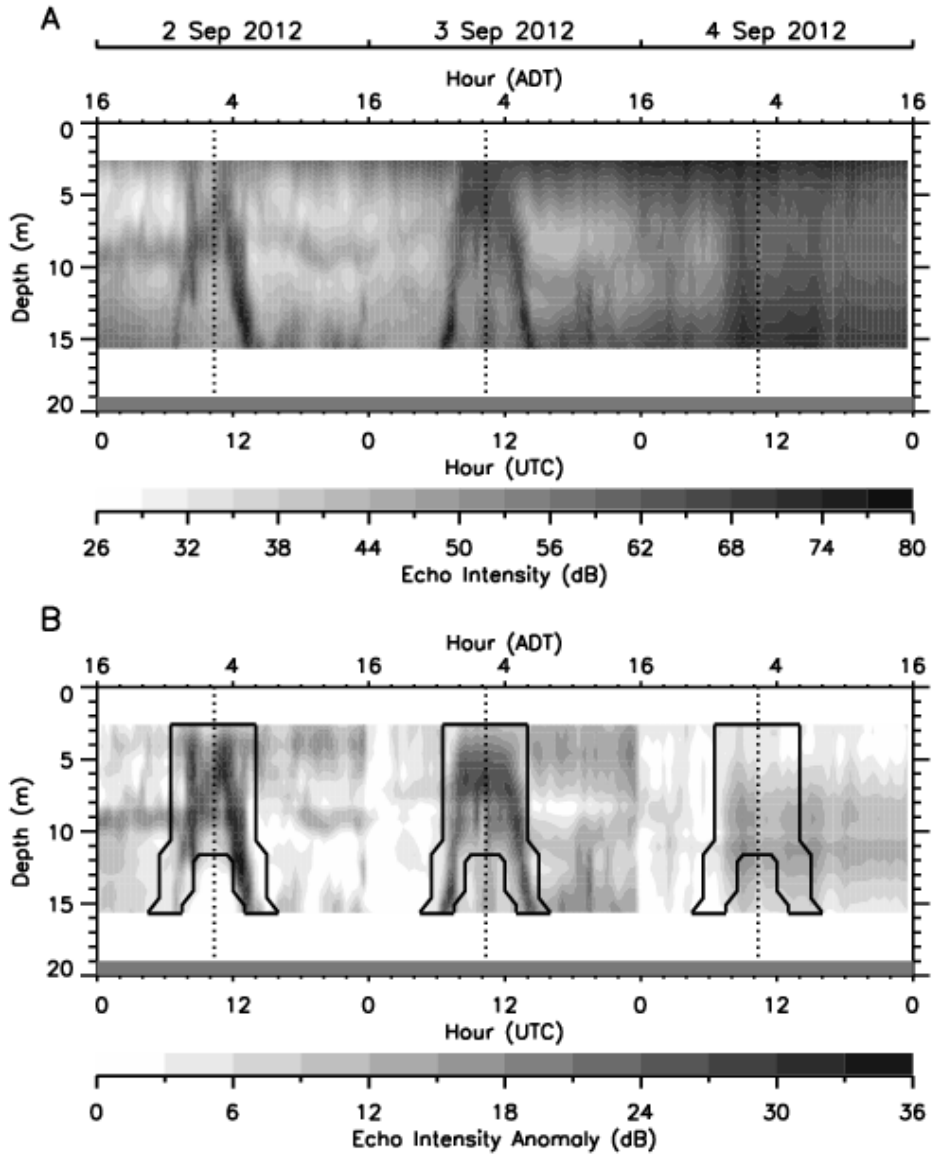

Figure 2 *A) Echo intensities for 2-4 September 2012. The vertical dotted lines correspond to local astronomical midnight, i.e. ~1020 UTC, ~0220 Alaska Daylight Time (ADT). B) Echo intensity anomalies for 2-4 September 2012. The thick black contour lines delineate DVM kernel values of 1 for local nighttime hours and 0 for daylight hours. Daily-mean wind speeds for 2-4 September are 5.8 m* s^{-1}*, 7.2 m* s^{-1} *and 10.0 m* s^{-1}*, respectively. The color version of this figure is included as a Supplementary figure.*

Their descent follows as daylight increases during the hours after local midnight. While there appears to be a DVM ascent trace on 4 September, a companion descent trace is not readily apparent. Also evident is a background signal that varies with depth and generally increases in

intensity over the depicted three-day period. This increasing background signal is related to turbulence in the water column that entrains scatterers from the bottom (presumably sediments and detritus) and air bubbles from the surface as daily wind speeds increase from 5.8 m s^{-1} on 2 September to 10.0 m s^{-1} on 4 September.

The echo intensities associated with this background signal incorporate the time-independent terms (C_1 and C_2) on the right hand side of equation 2 and echoes from scatterers (e.g. suspended sediments, detritus, air bubbles, non-migrating zooplankton; Gostiaux and van Haren, 2010) that don't exhibit DVM, but do vary slowly with time. Accordingly, the time series of echo intensities in each depth cell can be approximated as the sum of two principal signals: a short-period (daily) DVM-related signal and a long-period (multiple days) background signal.

$$I(t,z) = S_{vDVM}(t,z) + Background(t,z) \quad (3)$$

where

$$Background(t,z) = S_{vBACKGROUND}(t,z) + C_1 - C_2(z) \quad (4)$$

As stated above, our overall goal is to investigate whether temporal variability in DVM signals near Utqiaġvik encodes temporal variability of local and/or remote wind forcing. The strategy employed by Plueddemann and Pinkel (1989) to identify temporal variability in DVM signals was to compute echo intensity anomalies in individual depth cells by subtracting a time-averaged (13-day) echo intensity from the raw echo intensity data within each depth cell. At their deep

North Pacific Ocean study site, where ensonified depths ranged from 60 m to 1200 m, neither air bubbles nor suspended sediments contributed significantly to their measured echo intensities. As suggested by Figure 2A, which shows progressive increases in backscatter in near-surface and near-bottom waters, air bubbles and suspended sediments can contribute significantly to measured echo intensities on the shallow western Beaufort shelf. More importantly, the Plueddemann and Pinkel data were limited to a single season while our data were acquired in eight seasonal deployments over which non-DVM background scatterers exhibit considerable seasonal and interannual variability.

To account for these dynamic non-DVM background signals on the Beaufort shelf, we model the background signals as piecewise functions such that, for each of the forty-eight, 30-minute time steps t of a calendar day d, the background signal at depth z is taken to be the daily minimum in echo intensity at depth z for that calendar day.

$$Background(t,z) \approx min\{I_d(t=0:47,z)\} \quad (5)$$

The eight-season record of these background signals is significantly correlated with same day wind speeds (e.g. $r = 0.70, 0.39$ in the upper and lower depth bins, respectively; $p < 0.05$, two-tailed test, 28 degrees of freedom). After subtracting the modeled background signals from the measured echo intensities at each depth, an approximation of the daily DVM-related signal remains (Fig. 2B) and is encoded in the array of echo intensity anomalies, I'_d,

$$I'_d(t,z) = S_{vDVM}(t,z) \approx I_d(t,z) - min\{I_d(t=0:47,z)\}. \quad (6)$$

In essence, equation 6 represents a signal processing technique analogous to correcting for atmospheric haze in a satellite image of the earth's surface (e.g. Sabins, 1987); the effect of which is to increase the signal (DVM in the present context) to noise (other background scatterers) ratio. Our next step was to compute a single-valued daily index from echo intensities associated with DVM behavior, excluding echo intensities associated with non-migrating background scatterers. To do so, we empirically defined a kernel, K, with the same array dimensions as I'_d (i.e. 48 time steps x 27 depth bins). Kernel elements corresponding to a representative DVM signal, lying within the thick black outline depicted in Fig. 2B, were assigned a value of 1, whereas kernel elements not corresponding to the DVM signal (outside the thick black outline) were assigned a value of 0. Because the kernel and I'_d have the same array dimensions, a single-valued DVM index (DVMI) for day d then obtains from the convolution, $\otimes$, of I'_d and K, scaled by $1/N$, where N (= 418) is the number of value-1 elements of K:

$$DVMI(d) = \frac{1}{N} I'_d \otimes K \, . \qquad (7)$$

The resulting DVMIs for 2-4 September 2012 are 15.5, 16.4 and 8.6 dB, respectively. The full eight-season record of late-summer daily DVMIs (Fig. 3A) represents a working data set of krill (inferred biomasses) on the western Beaufort shelf.

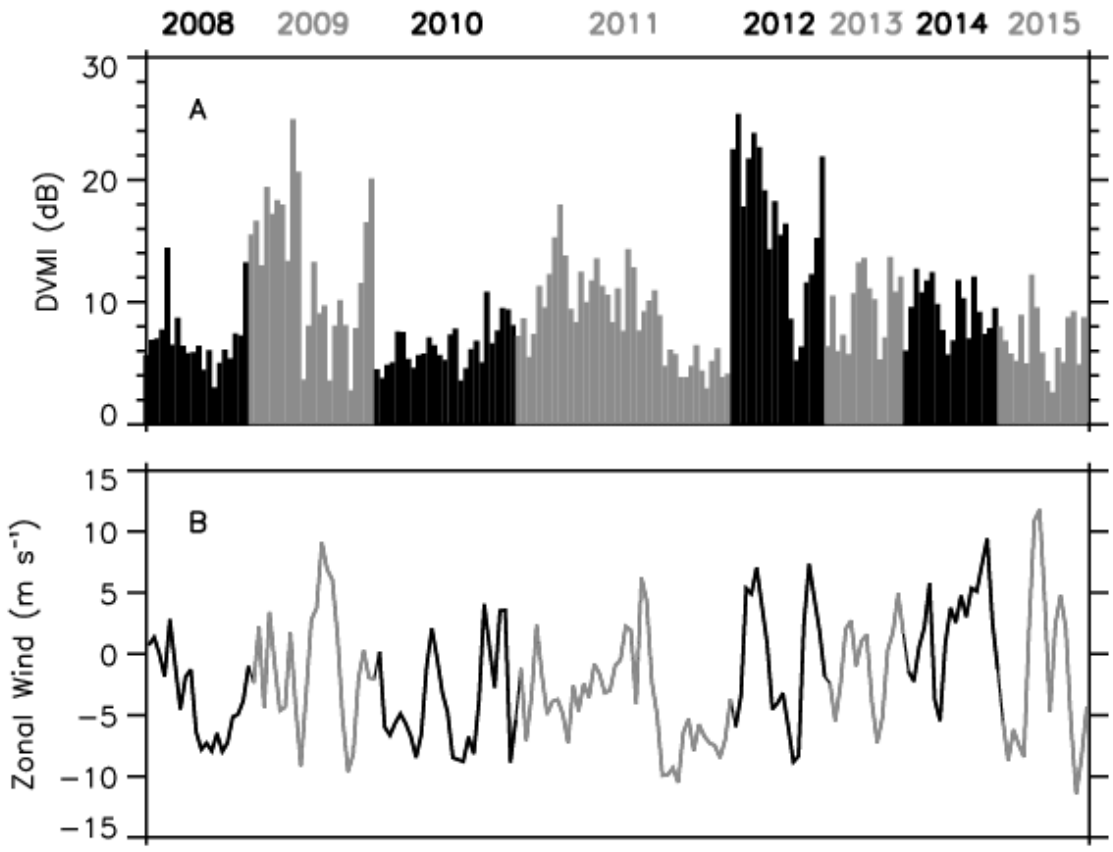

Figure 3 *A) Late-summer daily DVMIs for 2008-2015. See Supplementary Table 1 for seasonal start and end dates. B) Same-day local zonal winds.*

2.5 Daily DVMIs and an Upwelling Wind Threshold

In an idealized sense, the biophysical relationships among krill proxies on the western Beaufort shelf and local winds mentioned above represent a threshold model: krill are less available for efficient foraging by bowheads when easterly wind velocities exceed some threshold velocity, whereas krill are more available for efficient foraging when upwelling winds relax.

In comparing the daily DVMI record with same-day local zonal winds (Fig. 3A,B), a threshold relationship is suggested but not obvious. To identify the threshold in this relationship, we

created an array (Fig. 4A) from the irregularly-spaced data by bin averaging (smoothing) the daily DVMIs in 2 m s^{-1} bins (Rice Rule bin width estimate) advanced in 1 m s^{-1} steps for lags of 0 to 6 days (winds leading DVMIs); 6 days represents the mean decorrelation time scale for the eight seasonal DVMI time series. The largest gradient, ∂DVMI/∂U, in the array occurs for easterly winds at -6 m s^{-1} leading DVMI by one day (Fig. 4A). We interpret the maximum gradient as identifying a representative threshold upwelling wind velocity and the associated time lag as a representative time for the krill field to respond to a change in wind velocity across this threshold. We note that Sturges, Scott's and Freedman-Diaconis bin estimators yielded integer bin widths of 3 m s^{-1} and the upwelling threshold and time lag based on this bin averaging width were also -6 m s^{-1} and 1 day, respectively.

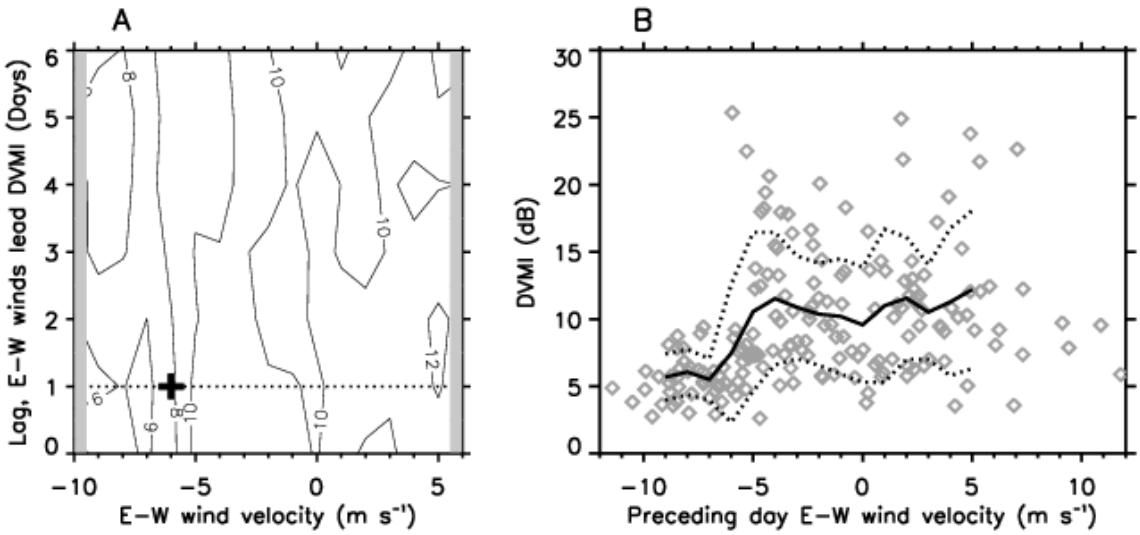

Figure 4 *A) Bin-averaged DVMIs vs leading E-W winds. Negative wind velocities identify winds from the east; positive wind velocities refer to winds from the west. Contour interval is 2 dB. The leading wind velocity at which the maximum gradient in averaged DVMIs occurs is indicated by the plus symbol. Gray shading indicates array elements for which less than eight individual DVMIs were averaged. Only averages computed from eight (= the standard deviation of the number of DVMIs used to compute all bin averages) or more DVMIs in each bin were retained. B) Individual preceding day zonal wind - DVMI pairs (diamonds) with running mean (black line) +/- 1 standard deviation corresponding to the horizontal dotted line in Figure 4A.*

347

348 *2.6 Interannual Variability in DVMIs*

349 The scatterplot of individual DVMI-wind pairs (at 1-day lag) and their bin-averaged mean
350 depicts upwelling and krill-trap biophysical states and the transitional threshold between them
351 (Fig. 4B). Seasonal mean DVMIs were computed for each of these states (Table 1) to reveal
352 interannual variability. Upwelling DVMIs vary little from year to year (4.77 to 6.42 dB),
353 whereas krill-trap DVMIs exhibit considerable interannual variability (6.74 to 17.94 dB).

354

355 ***Table 1*** *Seasonally-averaged DVMIs associated with upwelling and krill-trap wind conditions.*
356 *Units are dB. The numbers in parentheses refer to the number of daily DVMIs used to compute*
357 *each seasonal mean.*

	2008	2009	2010	2011	2012	2013	2014	2015	2008-2015
Upwelling	5.21 (7)	4.77 (3)	5.82 (10)	5.24 (13)	5.80 (2)	5.30 (1)	- (0)	6.42 (6)	5.51 (42)
Krill-Trap	7.93 (13)	14.06 (21)	6.74 (17)	10.42 (28)	17.94 (16)	9.90 (14)	9.36 (18)	7.09 (11)	10.43 (138)

358

359 To investigate the manner in which year-to-year differences in the time-integrated effects of
360 wind forcing over the Chukchi and Beaufort Seas are encoded as interannual differences in these
361 krill-trap DVMIs, we employed an iterative correlation analyses methodology adapted from
362 Okkonen et al., 2019. Specifically, iterative correlation analyses identify wind averaging periods
363 (start and end dates) that maximize the geographical extent over which correlations between
364 time-averaged NCEP winds and krill-trap DVMIs are statistically significant ($|r| > 0.707$, $p <$
365 0.05, two-tailed test, 6 degrees of freedom). Averaging period start and end dates were
366 constrained to fall within a window beginning 1 May, a representative start date for sea ice
367 retreat across the Chukchi Sea (Okkonen et al., 2019), and 11 September, the mean end date for
368 the mooring deployments. The relevant computer code, written in IDL

(https://www.harrisgeospatial.com/Software-Technology/IDL), is provided as Supplementary text.

3. Results

Aggregate results from the iterative correlation analyses suggest that differences in inferred late-summer krill biomasses at Utqiaġvik reflect differences in net responses to integrated wind forcing beginning over the Chukchi domain (9 July-11 August; Fig. 5A) that later transitions to wind forcing over the Beaufort domain (5-25 August; Fig. 5B).

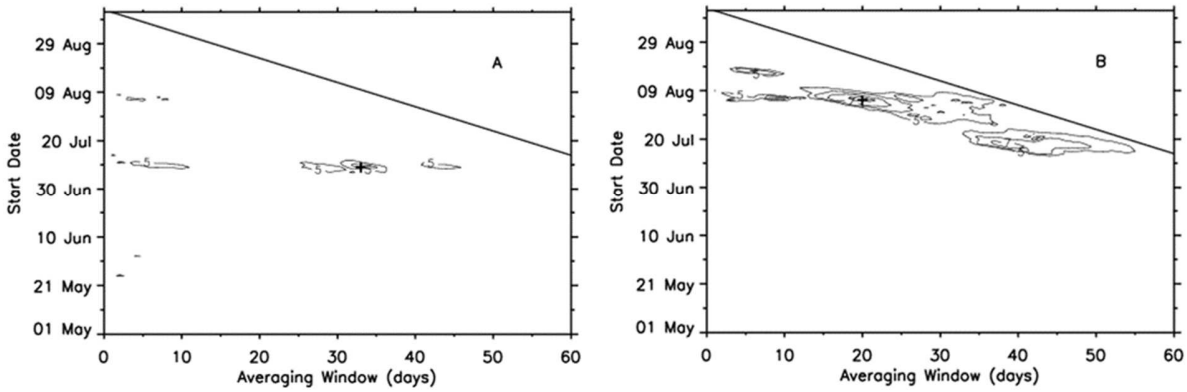

Fig. 5 *Contoured areas of the (A) Chukchi and (B) Beaufort domains over which the correlations between averaged (U, V) winds and krill-trap DVMIs are statistically significantly ($r > 0.707$, $p<0.05$; two-tailed test) versus averaging period and averaging start date. Contours at 5,6,7,8 x 10^5 km^2. For averaging periods greater than 60 days, there were no areas greater than 5 x 10^5 km^2 over which correlations were statistically-significant. The + symbols indicate the averaging coordinates for the maximum area in each plot. No results were computed for averaging period and start date pairs lying above the diagonal line because averaging period end dates are later than 11 September.*

We focus first on the average wind forcing regime over the Chukchi domain. In comparing mean mid-summer (9 July to 11 August) winds associated with years defined by positive krill-trap DVMI anomalies (2009 and 2012) with years defined by negative krill-trap DVMI anomalies (2008, 2010-2011, 2013-2015), it is immediately apparent that positive anomalies are predicated

on the occurrence of moderately constant (directional constancy ~0.4; gray scale shading, Fig. 6A) southerly winds over the Chukchi domain. The mean mid-summer SLP pattern driving these southerly winds (Fig. 6B) depicts a broad low pressure region over the western side of the Pacific-Arctic juxtaposed with high pressure regions over the eastern side. The north-south oriented isobars and resulting pressure gradient between the western and eastern SLP regimes dictate mean southerly winds over the Chukchi domain.

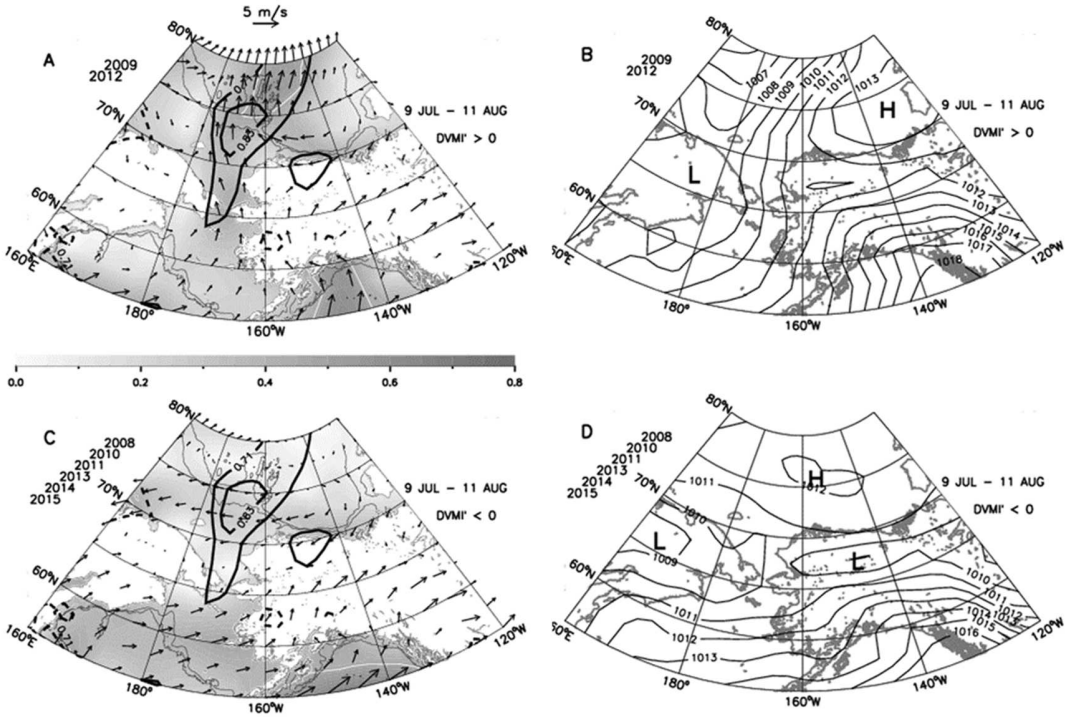

Fig. 6 *Mean atmospheric circulation from 9 July to 11 August for positive krill-trap DVMI anomaly years (A, B) and negative krill-trap DVMI anomaly years (C, D). A) and C) display mean wind vectors (at every 2nd ith grid point), wind directional constancy (gray scale shading) and statistically-significant correlations between DVMI and U-component winds (dashed black contours) and V-component winds (solid black contours) with correlation contours at r=0.707 (p < 0.05) and 0.834 (p < 0.01). White contour lines delineate directional constancy of 0.5. B) and D) display mean sea level pressure (hPa) patterns. High and low pressure cells are annotated with H and L, respectively. The color version of this figure is included as a Supplementary figure.*

In contrast, negative krill-trap DVMI anomalies are associated with weak, variable (i.e. low directional constancy) winds over the Chukchi domain and prevailing easterlies centered on

72.5°N (Fig. 6C), although these mid-summer zonal winds are not significantly correlated with DVMIs. This band of easterly winds extending across the Chukchi and Beaufort domains is the geostrophic response to the meridional pressure gradient residing between the weak high pressure cell in the northern portion of the Pacific-Arctic region and the weak, broad low pressure region (~1010 hPa) extending across Russian and Alaskan land masses (Fig. 6D).

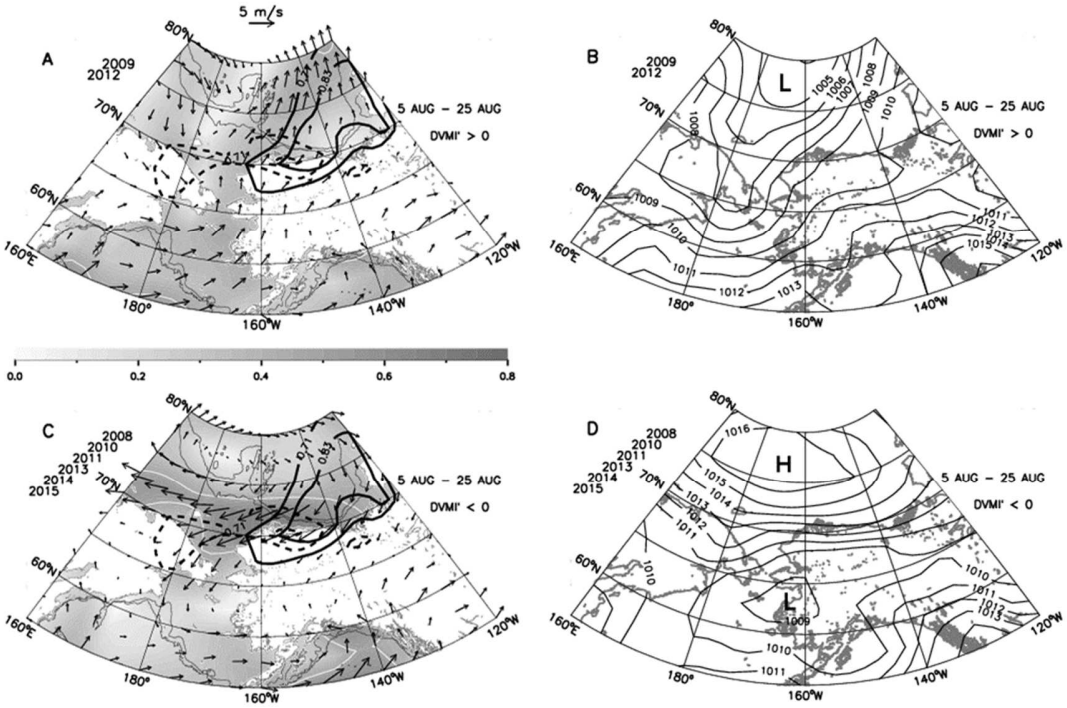

Fig. 7 *Same as Fig. 6 only mean atmospheric circulation from 5 August to 25 August. The color version of this figure is included as a Supplementary figure.*

By late-summer (5 August to 25 August), statistically-significant correlations between average winds and krill-trap DVMIs occupy a broad region extending from the northern Chukchi shelf to the Alaskan Beaufort coast and Canadian archipelago (Figure 7). Positive krill-trap DVMI anomalies are associated with generally weak southwesterly winds over the northern Chukchi shelf and weak southerly winds over the Beaufort domain (Fig. 7A). The mean SLP pattern giving rise to this late-summer wind regime results from a deepening and eastward migration of

426 the weak low pressure region that occupied the western portion of the Pacific-Arctic in mid-
427 summer (cf. Fig. 6B) to become a well-defined low pressure trough extending from the Bering
428 Strait northward across the Chukchi Sea (Fig. 7B). Negative krill-trap DVMI anomalies are
429 associated with strong and relatively constant (> 0.5), late-summer easterly winds over the
430 southern Beaufort and northern Chukchi Seas (Fig. 7C). These energetic easterly winds reflect an
431 intensified pressure gradient between a stronger high pressure cell over the northern Chukchi and
432 Beaufort domains and a broad low pressure region over the central Alaskan landmass (Fig. 7D).
433

434 **4. Discussion**

435

436 We have shown that a multiyear record of indices (DVMI) derived from acoustic observations of
437 diel vertical migration encodes aspects of the temporal, geographic and amplitude characteristics
438 of wind forcing regimes that influence krill biomass potentially available to foraging bowhead
439 whales on the western Beaufort shelf.
440

441 Our DVMI-based upwelling wind velocity threshold (U = -6 m s^{-1}) and one-day lagged response
442 estimates agree well with upwelling characterizations based on changes in salinity recorded by a
443 nearby Beaufort Sea shelf break mooring array (Schulze and Pickart, 2012) and on changes in
444 ocean current velocities measured at the western end of the Beaufort shelf (Okkonen et al.,
445 2011). As a check on how data from 2009 and 2012 influenced the determination of the -6 m s^{-1}
446 upwelling threshold, DVMIs were again bin-averaged in association with their prior zonal wind
447 histories, but this time excluding 2009 and 2012 data. The result was that the upwelling threshold

448 occurred at -5 m s^{-1} with the inferred krill aggregation response time remaining at a lag of one
449 day.
450
451 The persistent plateau of elevated DVMIs many days after upwelling winds relax (Fig. 4A) is
452 consistent with the observations reported by Ashjian et al. (2010) who noted that bowhead whale
453 groups and numbers on the western Beaufort shelf were larger two to three days after
454 occurrences of easterly, upwelling-favorable winds. Furthermore, results showing that krill-trap
455 DVMIs are larger than upwelling DVMIs (Table 1) are consistent with the krill trap conceptual
456 model and other krill proxies (Ashjian et al., 2010; Okkonen et al., 2011; Shelden and Mocklin,
457 2013). The finding that years with the smallest krill-trap DVMIs occur when late-summer
458 easterly upwelling winds over the Alaskan Beaufort shelf are more persistent, with few
459 relaxation events, (Table 1) also supports the krill trap conceptual model in that krill, even if
460 abundant, are not as likely to be retained and aggregated on the shelf without relaxation of
461 upwelling winds.
462
463 Correlation analyses indicating that the largest DVMIs occurred in years (2009 and 2012) when
464 mean mid-summer winds over the Chukchi Sea were southerly (Fig. 6) agree with numerical
465 particle tracking experiment results that associated elevated krill abundances near Utqiaġvik in
466 autumn with earlier southerly winds over the Chukchi Sea (Berline et al., 2008). These results
467 also are consistent with the modeling of Chapman and Winsor (2004) who demonstrated that,
468 under southerly winds, most of the Pacific Water entering the Chukchi Sea through Bering Strait
469 converges near Utqiaġvik. Given that the krill in the Chukchi Sea are believed to originate in the
470 Bering Sea and are then transported in the dominant currents northward, the dependence of

471 DVMI on wind conditions and broad–scale atmospheric forcing suggests that southerly winds
472 either hasten the annual transport of krill to the Utqiaġvik region or result in most of the krill that
473 enter in the Chukchi in the Pacific Water arrive at Utqiaġvik in autumn.
474
475 Different methodologies for computing DVMI were explored. We modeled the daily background
476 signal in each depth cell as a linear trend and bias spanning the DVM kernel. Because the
477 resulting daily DVMIs were linearly related (r = 0.85) with DVMIs calculated using Eq. 5 (recall
478 that correlation does not depend on the scale of the variables), the results of the subsequent wind-
479 related analyses were not markedly different than those predicated on modeling the background
480 signal as daily minimum echo intensities; the threshold upwelling wind velocity was -6 m s^{-1} and
481 the inferred zooplankton response was nearly equal for lags of one and two days. We also
482 alternately defined daily DVMIs as equal to the largest echo intensity occurring within the DVM
483 kernel instead of according to equation 6. These two versions of the DVMI time series were also
484 linearly related (r = 0.85) and the results of the wind-related analyses based on the alternate
485 DVMI time series were not appreciably different than those presented in Figures 4-7.
486
487 The biomass of krill near Utqiaġvik also could depend on interannual variability in krill
488 recruitment in the Bering Sea or on the dominant life stage at which krill reach the northern
489 Chukchi Sea that in turn could depend on their pathway of advection, given that older, larger
490 krill would have greater individual biomass than younger, smaller krill. Krill in the Bering Sea
491 are believed to have 3-4 year life spans (H.R. Harvey, pers. comm.), suggesting that older life
492 stages found in the northern Chukchi may have experienced longer transit times, arriving via the
493 western advective pathway. High biomass also could result from abundant smaller, younger

494 furcilia life stages, suggesting good recruitment in the Bering Sea during that year with direct
495 transport to the northern Chukchi via an eastern advective pathway. The interdependencies of
496 variability in recruitment, in advective pathways, and in dominant life stages are beyond the
497 scope of the present analysis yet the observed associations pose intriguing questions and
498 highlight the potential importance of krill dynamics in the upstream source region (Bering Sea).
499
500 We speculate that the Utqiaġvik area may diminish in importance as a core use area during the
501 bowheads' fall migration. This speculation is based on our results that associate relatively poorer
502 foraging opportunities for bowheads in this core use area with strong, easterly winds over the
503 Beaufort shelf (Fig. 7C) and the reported increasing trend in easterly wind speeds over the
504 Beaufort region (Stegall and Zhang, 2012; Pickart et al., 2013) attributable to diminishing Arctic
505 sea ice cover (Comiso et al., 2008; Polyakov et al., 2012). The availability of krill at Utqiaġvik
506 depends also on the upstream supply; continued ocean warming of the Bering Sea may result in
507 diminished krill populations there and a reduced supply to the northern Chukchi Sea.
508
509 **5. Conclusions**
510
511 We used daily and seasonally-averaged indices derived from acoustic observations of krill diel
512 vertical migration to diagnose intra-seasonal and interannual relationships among the late-
513 summer krill field on the western Beaufort shelf and local and regional wind regimes. The
514 threshold wind speed at which easterly winds promote upwelling of krill onto the western
515 Beaufort shelf is ~6 m s^{-1}. Years in which inferred late-summer krill biomasses were relatively
516 high occurred when time-averaged mid-summer winds over the Chukchi Sea were from the

south and late-summer averaged winds over the Beaufort shelf were weak; wind conditions that promote more rapid advection of krill across the Chukchi shelf and subsequent retention of krill on the western Beaufort shelf. Years in which inferred late-summer krill biomasses were relatively low occurred when mid-summer meridional winds over the Chukchi Sea were weak and late-summer winds over the Beaufort shelf were easterly and strong; wind conditions associated with slower advection of krill across the Chukchi shelf and non-retention of krill on the western Beaufort shelf.

Acknowledgments

We are grateful to the many people and organizations who contributed to the success of this work. In particular, we are grateful to Dave Leech and Pete Shipton for their technical expertise in support of the mooring program. We also thank Eugene Brower and the Barrow Whaling Captains Association, the Alaska Eskimo Whaling Commission, North Slope Borough Mayors George Ahmaogak and Edward Itta, and the North Slope Borough Department of Wildlife Management including Taqulik Hepa, Harry Brower Jr., Robert Suydam, Billy Adams, Cyd Hanns, Leslie Pierce, and especially Craig George. The work would not have been possible without the experience and assistance of Bill Kopplin, the captain of the R/V Annika Marie and R/V Ukpik, and crew members Ned Manning, Mike Johnson, Randy Pollock, Tony D'Aoust, Mike Fleming, Lars Isaac, and Johnny Bjorgaard. Logistics at Utqiaġvik and Prudhoe Bay were provided by Glenn Sheehan, Lewis Brower, the Barrow Arctic Science Consortium, UIC Science, Polar Field Services, and British Petroleum. Thanks to our colleagues and collaborators with whom we worked in Utqiaġvik including Janet Clarke, Megan Ferguson, Dave Rugh, Kim Shelden, Mark Baumgartner, Barry Sherr, and Ev Sherr. This research was supported by the National Science Foundation through grants PLR-1023331 and OPP-0436131 to C. J. Ashjian, PLR-1022139 and OPP-0436110 to R. G. Campbell, and PLR-1023446 and OPP-043166 to S. R. Okkonen and with funds from the National Oceanic and Atmospheric Administration (NOAA) under cooperative agreement NA08OAR4320751 with the University of Alaska and cooperative agreements NA17RJ1223 and NA09OAR4320129 with the Woods Hole Oceanographic Institution. Support was also provided by the Minerals Management Service (MMS), now Bureau of Ocean Energy Management (BOEM), through Interagency Agreement 0106RU39923 / M08PG20021 between the National Marine Fisheries Service and MMS/

BOEM and through the National Oceanographic Partnership Program with award number N00014-08-1-0311 from the Office of Naval Research to the Woods Hole Oceanographic Institution. Additional support was provided by the Coastal Marine Institute at the University of Alaska the James M. and Ruth P. Clark Arctic Research Initiative Fund at the Woods Hole Oceanographic Institution. This is contribution #7 from the Scholarly Union of Bio-Physical Arctic Researchers.

586 **References**

587

588 Ashjian, C.J., Smith, S.L., Flagg, C.N., Wilson, C., 1998. Patterns and occurrence of diel vertical
589 migration of zooplankton biomass in the Mid-Atlantic Bight described by an acoustic Doppler
590 current profiler. Continental Shelf Research 18, 831–858.
591
592 Ashjian, C.J., Smith, S.L., Flagg, C.N., Mariano, A.J., Behrens, W.J., Lane, P.V.Z., 1994. The
593 influence of a Gulf Stream meander on the distribution of zooplankton biomass in the Slope
594 Water, the Gulf Stream, and the Sargasso Sea, described using a shipboard acoustic Doppler
595 current profiler. Deep-Sea Research I 41, 23–50.
596
597 Ashjian, C.J., Braund, S.R., Campbell, R.G., George, J.C., Kruse, J., Maslowski, W., Moore,
598 S.E., Nicolson, C.R., Okkonen, S.R., Sherr, B.F., Sherr, E.B., Spitz, Y., 2010. Climate
599 Variability, Oceanography, Bowhead Whale Distribution, and Iñupiat Subsistence Whaling near
600 Barrow, AK. Arctic, 63(2):179-194.
601
602 Ashjian, C.J., Campbell, R.G., Okkonen, S.R., Alatalo, P. 2013. Year-to-year variability of krill
603 abundance at a bowhead whale feeding hotspot near Barrow, AK: 2005-2012. Alaska Marine
604 Science Symposium. January 21-25, 2013. Anchorage, Alaska.
605
606 Berge, J., Cottier, F., Last, K.S., Varpe, Ø., Leu, E., Søreide, J., Eiane, K., Falk-Petersen, S.,
607 Willis, K., Nygard, H., Vogedes, D., Griffiths, C., Johnsen, G., Lorentzen, D., Brierley, A.S.
608 2009. Diel migration of Arctic zooplankton during the polar night. Biol. Let. 5:69-72.
609 doi:10.1098/rsbl.2008.0484
610
611 Berline, L., Spitz, Y.H., Ashjian, C.J., Campbell, R.G., Maslowski, W., Moore, S.E., 2008.
612 Euphausiid transport in the western Arctic Ocean. Mar. Ecol. Progress. Ser. 360,163–178.
613
614 Brugler, E.T., Pickart, R.S., Moore, G.W.K., Roberts, S., Weingartner, T.J., Statscewich, H.,
615 2014. Seasonal to interannual variability of the Pacific water boundary current in the Beaufort
616 Sea. Prog. Oceanogr. 127, 1−20. https://doi.org/10.1016/j.pocean.2014.05.002.
617
618 Citta, J.J., Quakenbush, L.T., George, J.C., Small, R.J., Heide-Jorgensen, M.P., Brower, H.,
619 Adams, B., Brower, L., 2012. Winter movements of bowhead whales (Balaena mysticetus) in the
620 Bering Sea. Arctic 65, 13–34.
621
622 Comiso, J.C., Parkinson, C.L., Gersten, R., Stock, L., 2008. Accelerated decline in the Arctic sea
623 ice cover. Geophys. Res. Lett., 35, L01703, doi:10.1029/2007GL031972.
624
625 Cottier, F.R., Tarling, G.A., Wold, A., Falk-Petersen, S. 2006. Unsynchronized and synchronized
626 vertical migration of zooplankton in a high arctic fjord. Limnol. Oceanogr. 51(6), 2586–2599.
627
628 Deines, K.L. 1999. Backscatter estimation using broadband acoustic Doppler current profilers.
629 Proc. Sixth Working Conf. on Current Measurement, San Diego, CA, IEEE. 249-253.

Flagg, C.N., Smith, S.L. 1989. On the use of the acoustic Doppler current profiler to measure zooplankton abundance. Deep-Sea Res 36(3): 455-474

Gostiaux, L., van Haren, H., 2010. Extracting meaningful information from uncalibrated backscattered echo intensity data. J. Atmos. Oceanic Tech. 27:943-949, doi: 10.1175/2009JTECHO704.1

Heywood, K.J. 1996. Diel vertical migration of zooplankton in the Northeast Atlantic. J. Plankton Res. 18(2), 163-184.

Kalnay, E., Kanamitsu, M., Kistler, R., Collins, W., Deaven, D., Gandin, L., Iredell, M., Saha, S., White, G., Woollen, J., Zhu, Y., Leetmaa, A., Reynolds, R., Chelliah, M., Ebisuzaki, W., Higgins, W., Janowiak, J., Mo, K.C., Ropelewski, C., Wang, J., Jenne, R., Joseph, D., 1996. The NCEP/NCAR 40-year reanalysis project. Bulletin of the American Meteorological Society 77, 437–470.

Lawson, G.L., Wiebe, P.H., Ashjian, C.J., Gallager, S.M., Davis, C.S., Warren, J.D., 2004. Acoustically-inferred zooplankton distribution in relation to hydrography west of the Antarctic Peninsula. Deep-Sea Res. II, 51:2041–2072.

Mocklin, J.A., Rugh, D.J, Moore, S.E., Angliss, R.P. 2011. Using aerial photography to investigate evidence of feeding by bowhead whales. Marine Mammal Sci. 28(3): 602–619. doi: 10.1111/j.1748-7692.2011.00518.x

Moore, G.W.K., 2003. Gale force winds over the Irminger Sea to the East of Cape Farewell Greenland. Geophys. Res. Lett. 30, 184–187.

Moore, S.E., Reeves, R.R., 1993. Distribution and movement. In: Burns, J.J., Montague, J.H., Cowles, C.J. (Eds.), The bowhead whale, Special Publication Number 2, The Society for Marine Mammalogy. Allen Press Inc., Lawrence, KS, pp. 313–386.

Moore, S.E., DeMaster, D.P., Dayton, P.K., 2000. Cetacean habitat selection in the Alaskan Arctic during summer and autumn. Arctic 53:432–447.

Okkonen, S.R., Ashjian, C.J., Campbell, R.G., Clarke, J.T., Moore, S.E., K.D. Taylor, K.D., 2011. Satellite observations of circulation features associated with a bowhead whale feeding 'hotspot' near Barrow, Alaska. Remote Sensing of Environment 115:2168-2174.

Okkonen, S.R., C.A. Ashjian, R.G. Campbell, P. Alatalo. 2019. The encoding of wind forcing into the Pacific Arctic pressure head, Chukchi Sea ice retreat and late-summer Barrow Canyon water masses. Deep-Sea Research Part II, 162:22-31. doi.org/10.1016/j.dsr2.2018.05.009

Pickart, R.S., Moore, G.W.K., Torres, D.J., Fratantoni, P.S., Goldsmith, R.A., Yang, J., 2009. Upwelling on the continental slope of the Alaskan Beaufort Sea: Storms, ice, and oceanographic response. Journal of Geophysical Research, 114, C00A13, doi:10.1029/2008JC005009.

Pickart, R.S., Schulze, L.M., Moore, G.W.K., Charette, M.A., Arrigo, K.R., van Dijken, G., Danielson, S.L., 2013. Long-term trends of upwelling and impacts on primary productivity in the Alaskan Beaufort Sea. Deep Sea Res. Part I, 79:106–121, doi.org/10.1016/j.dsr.2013.05.003.

Plueddemann, A.J., Pinkel, R., 1989. Characterization of the patterns of diel migration using a Doppler sonar. Deep-Sea Res., 36:509-530.

Polyakov, I. V., Kwok, R., Walsh, J.E., 2012. Recent changes of arctic multiyear sea-ice coverage and the likely causes. Bull. Amer. Meteor. Soc., 93, 145–151.

Sabins, F.F. 1987. Remote Sensing: Principles and Interpretation. ISBN 0-7167-1793-X., W.H. Freeman and Co., New York. 443 pp.

Schulze, L. M., Pickart, R.S., 2012. Seasonal variation of upwelling in the Alaskan Beaufort Sea: Impact of sea ice cover, J. Geophys. Res., 117, C06022, doi:10.1029/2012JC007985.

Shelden, K.E.W. and Mocklin, J.A., Editors. 2013. Bowhead Whale Feeding Ecology Study (BOWFEST) in the western Beaufort Sea. Final Report, OCS Study BOEM 2013-0114. National Marine Mammal Laboratory, Alaska Fisheries Science Center, NMFS, NOAA, 7600 Sand Point Way NE, Seattle, WA 98115-6349.

Smoot, C.A., Hopcroft, R.R., 2016. Cross-shelf gradients of epipelagic zooplankton communities of the Beaufort Sea and the influence of localized hydrographic features. J. Plankt. Res. 39: 79-91.

Sourisseau M, Simard Y, Saucier F.J. 2008. Krill diel vertical migration fine dynamics, nocturnal overturns, and their roles for aggregation in stratified flows. Can. J. Fish. Aquat. Sci. 65: 574–587.

Spall, M.A., 2007. Circulation and water mass transformation in a model of the Chukchi Sea. J. Geophys. Res. 112, C05025.

Stegall, S.T., Zhang, J., 2012. Wind Field Climatology, Changes, and Extremes in the Chukchi–Beaufort Seas and Alaska North Slope during 1979–2009. J. Climate, 25:8075-8089. doi.org/10.1175/JCLI-D-11-00532.1

Tarling, G.A., Jarvis, T., Emsley, S.M., Matthews, J.B.L. 2002. Midnight sinking behaviour in Calanus finmarchicus: A response to satiation or krill predation? Mar. Ecol. Prog. Ser. 240: 183–194.

Winsor, P., Chapman, D.C., 2004. Pathways of Pacific water across the Chukchi Sea: a numerical model study. J. Geophys. Res. 109 (C3), C03002. doi.org/10.1029/2003JC001962.

Supplementary Material

Table S1 Mooring deployment details

Year	Location	Deployment Times/dates UTC	Complete days	Sample Interval
2008	71° 13.752'N 154° 31.548'W	0132 20 Aug 2334 10 Sep	20	15 min
2009	71° 21.096'N 155° 13.777'W	2223 21 Aug 2118 15 Sep	24	15 min
2010	71° 21.085'N 155° 13.691'W	0415 19 Aug 2324 16 Sep	27	20 min
2011	71° 21.069'N 155° 13.752'W	2348 18 Aug 2320 29 Sep	41	20 min
2012	71° 21.031'N 155° 13.564'W	2251 23 Aug 2350 11 Sep	18	15 min
2013	71° 21.034'N 155° 13.493'W	2324 17 Aug 1750 02 Sep	15	20 min
2014	71° 21.040'N 155° 13.560'W	2148 19 Aug 1616 07 Sep	18	15 min
2015	71° 21.026'N 155° 13.434'W	1902 20 Aug 1608 07 Sep	17	15 min

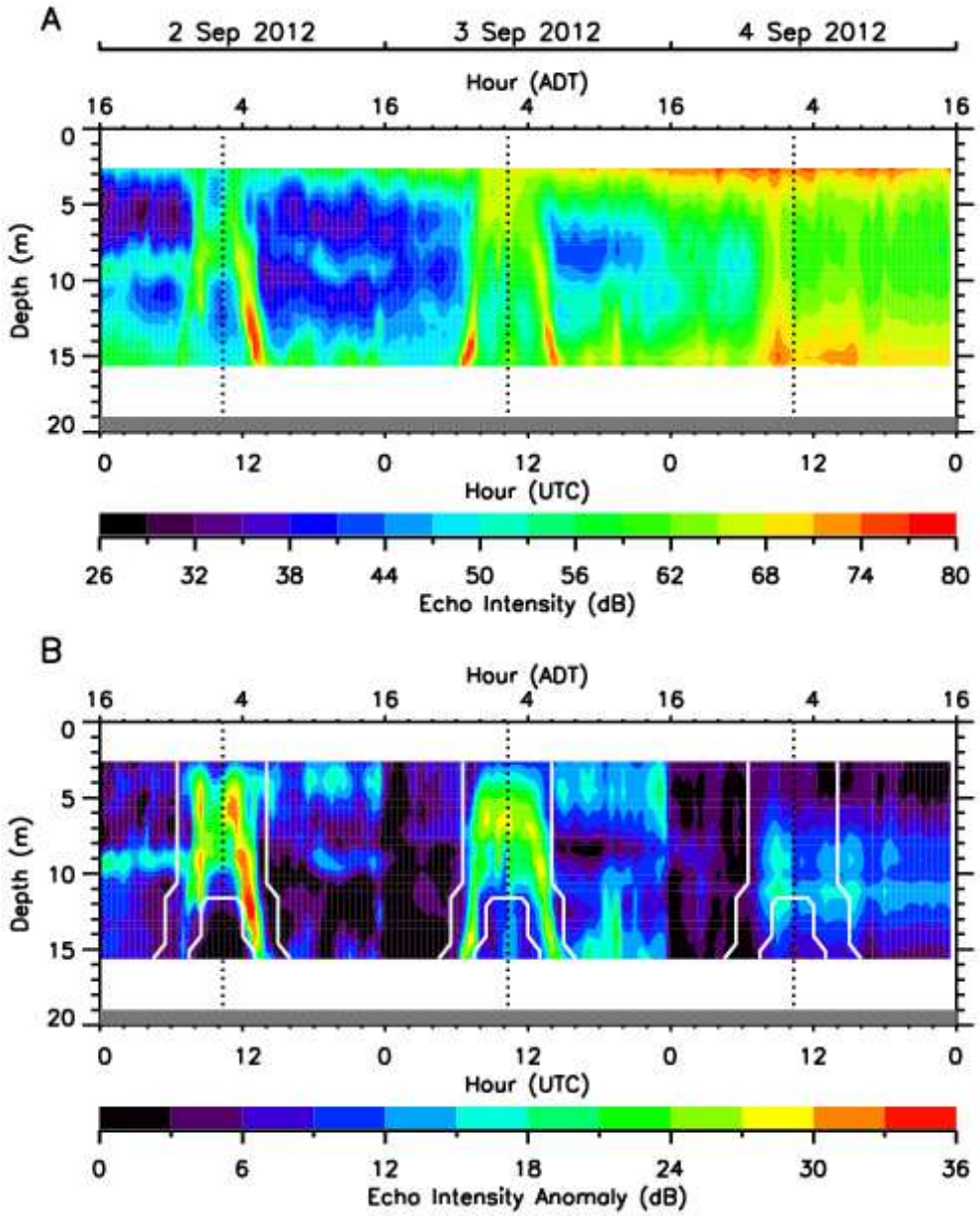

Figure 2 *A) Echo intensities for 2-4 September 2012. The vertical dotted lines correspond to local astronomical midnight, i.e. ~1020 UTC, ~0220 Alaska Daylight Time (ADT). B) Echo intensity anomalies for 2-4 September 2012. The thick white contour lines delineate DVM kernel values of 1 for local nighttime hours and 0 for daylight hours. Daily-mean wind speeds for 2-4 September are 5.8 m* s^{-1}*, 7.2 m* s^{-1} *and 10.0 m* s^{-1}*, respectively.*

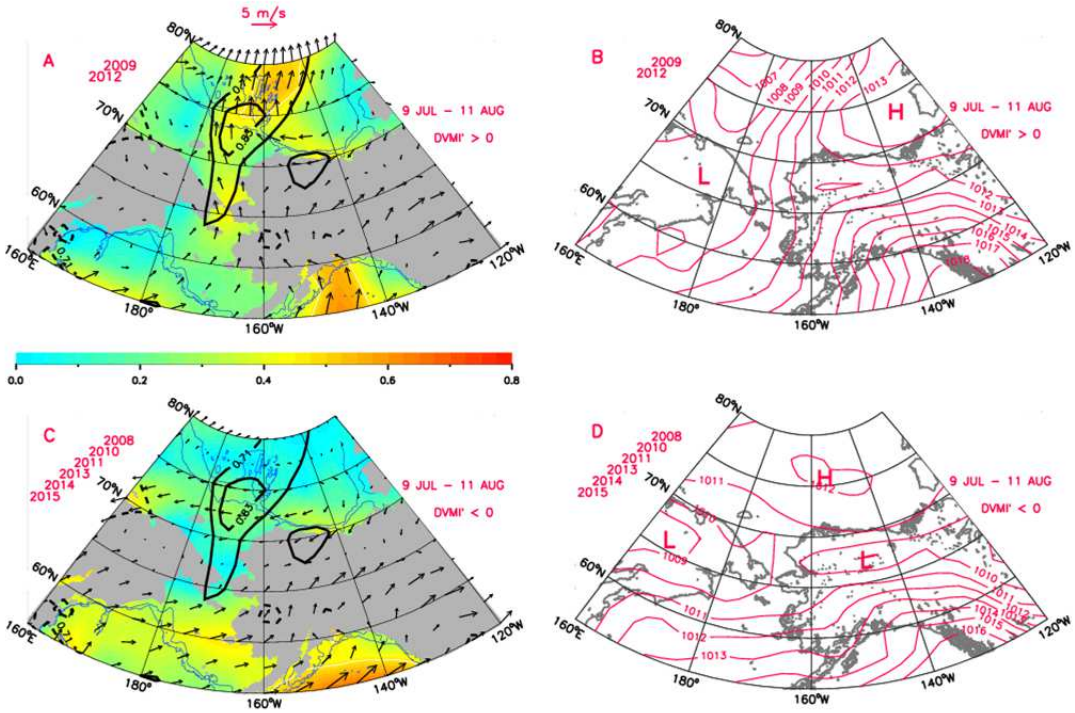

Fig. 6 *Mean atmospheric circulation from 9 July to 11 August for positive krill-trap DVMI anomaly years (A, B) and negative krill-trap DVMI anomaly years (C, D). A) and C) display mean wind vectors (at every 2nd ith grid point), wind directional constancy (color shading) and statistically-significant correlations between DVMI and U-component winds (dashed black contours) and V-component winds (solid black contours) with correlation contours at r=0.707 (p < 0.05) and 0.834 (p < 0.01). White contour lines delineate directional constancy of 0.5. B) and D) display mean sea level pressure (hPa) patterns. High and low pressure cells are annotated with H and L, respectively.*

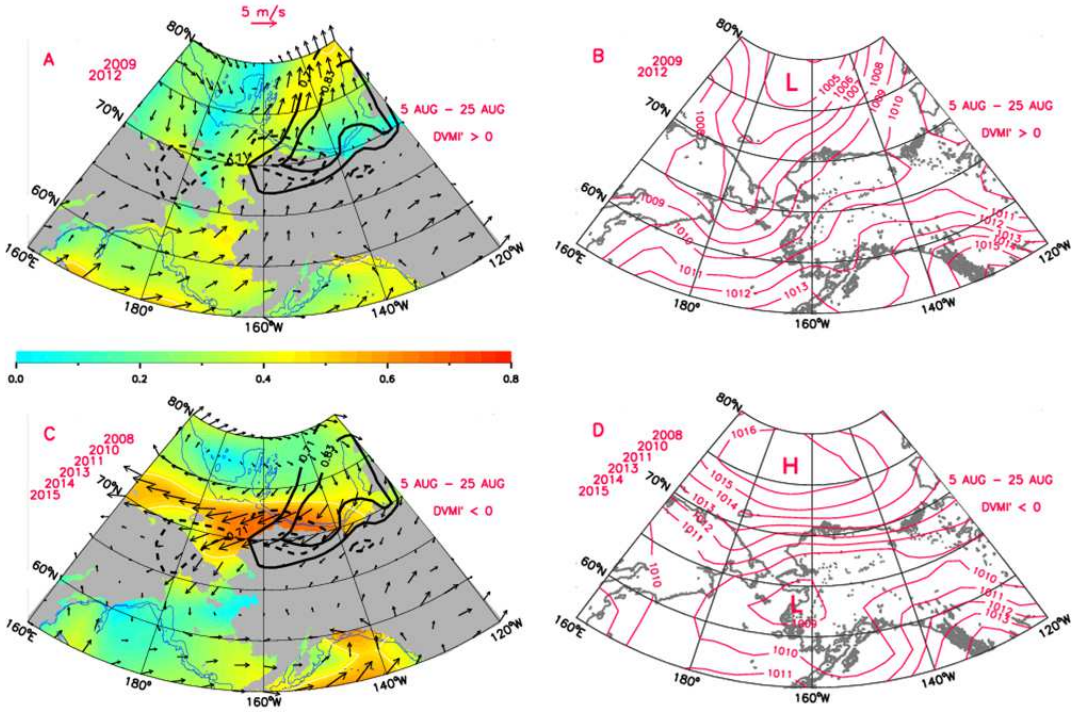

Fig. 7 *Same as Fig. 6 only mean atmospheric circulation from 5 August to 25 August.*

IDL code for iterative correlation analyses

```
;krill-trap DVMIs for 2008-2015; see Table 1
dvmi=[7.93,14.06,6.74,10.42,17.94,9.90,9.36,7.09]

for aperiod=1,134 do begin                ;averaging periods (days)

  for sdoy=121,255-aperiod do begin       ;DOY start dates 1 May-11 Sep

    for ix=0,32 do begin                  ;NCEP longitude indices, 160°E-120°W

      for iy=0,6 do begin                 ;NCEP latitude indices, 80°N-65°N

        for dyr=2008,2015 do begin        ;DVMI and wind year

          ;identify NCEP time series index (windx) corresponding to
          ;year and start date
          ;uwind, vwind, windyr and winddoy are obtained from the NCEP
          ;data
          windx=where(windyr eq dyr and winddoy eq sdoy)

          ;for each year, compute mean U and V winds at each NCEP
          ;location for the current averaging period and start date
          muu(dyr)=mean(uwind(ix,iy,windx:windx+aperiod-1))
          mvv(dyr)=mean(vwind(ix,iy,windx:windx+aperiod-1))
        endfor                            ;dyr loop

        ;compute correlation coefficients, ru and rv
        ru(ix,iy)=correlate(muu,dvmi)     ;U x DVMI
        rv(ix,iy)=correlate(mvv,dvmi)     ;V X DVMI
      endfor                              ;iy loop

    endfor                                ;ix loop

    ;identify oceanic NCEP locations in the Chukchi and Beaufort
    ;domains where ru and rv are statistically significant
    cuv=where(chukchi eq 1 and (ru gt 0.707 or rv gt 0.707))
    buv=where(beaufort eq 1 and (ru gt 0.707 or rv gt 0.707))

    ;if there is at least one oceanic NCEP location where the
    ;correlation is significant, then compute the total oceanic areas
    ;in the Chukchi and Beaufort domains over which correlations are
    ;significant
    if(total(cuv) gt 0.)then acuv(aperiod,sdoy)=total(area(cuv))
    if(total(buv) gt 0.)then abuv(aperiod,sdoy)=total(area(buv))

  endfor                                  ;sdoy loop
endfor                                    ;aperiod loop

acuv=acuv(1:134,121:254)
abuv=abuv(1:134,121:254)
```

```
845
846   ;identify the indices (averaging period and start date) for which the
847   ;area of statistically-significant correlations is maximum
848
849   maxc=max(acuv,mc)
850   avgc=mc mod 134    ;identify averaging period index Chukchi domain
851   startc=mc/134      ;identify start date index Chukchi averaging period
852
853   maxb=max(abuv,mb)
854   avgb=mb mod 134    ;identify averaging period index Beaufort domain
855   startb=mb/134      ;identify start date index Beaufort averaging period
856
857   ;averaging period indices 0,1,2,…,133 correspond to averaging periods
858   1,2,3,…,134 days
859
860   ;start date indices 0,1,2,…,133 correspond to start dates 1 May,2
861   May,3 May,…,11 Sep
862
```